ISSN 1063-7761, Journal of Experimental and Theoretical Physics, 2018, Vol. 126, No. 5, pp. 660–665. © Pleiades Publishing, Inc., 2018.
Original Russian Text © Yu.E. Samoshkina, A. Rogalev, 2018, published in Zhurnal Eksperimental'noi i Teoreticheskoi Fiziki, 2018, Vol. 153, No. 5, pp. 794–799.

ORDER, DISORDER, AND PHASE TRANSITION IN CONDENSED SYSTEM

Electronic and Magnetic States of Pr and Mn in the $Pr_{1-x}Sr_xMnO_3$ Films Studied by XANES and XMCD Spectroscopy

Yu. E. Samoshkina[a,*] **and A. Rogalev**[b]

[a] *Kirensky Institute of Physics, Federal Research Center "Krasnoyarsk Scientific Center," Siberian Branch, Russian Academy of Sciences, Krasnoyarsk, 660036 Russia*

[b] *European Synchrotron Radiation Facility, Grenoble, CS 40220 38043 France*

**e-mail: uliag@iph.krasn.ru*

Received November 16, 2017

Abstract—The spectral dependences of X-ray absorption near-edge spectroscopy (XANES) and X-ray magnetic circular dichroism (XMCD) and the field dependences of XMCD near the K edge of Mn and the $L_{2,3}$ edges of Pr in the $Pr_{0.8}Sr_{0.2}MnO_3$ and $Pr_{0.6}Sr_{0.4}MnO_3$ films at $T = 90$ K are studied. The spectral dependences point to a mixed valence state of Mn and Pr in the films. It is found that, as compared to XANES, XMCD is more sensitive to the valence state of Pr^{4+}. The field dependences of XMCD point to ferromagnetic behavior of Mn ions and the Van Vleck paramagnetism of Pr ions, which makes a significant contribution to the total magnetization of the films. It is shown that as the Sr concentration increases, the XMCD intensity at the K edge of Mn increases, which indicates a growth of the total magnetic moment of the film due to an increase in the $4p$–$3d$ hybridization.

DOI: 10.1134/S1063776118040131

1. INTRODUCTION

Substituted $Ln_{1-x}A_xMnO_3$ (Ln is lanthanide, A is alkaline earth ion) manganites are unique compounds exhibiting various magnetic and transport properties [1–3], and many of them are used in practice. Owing to further possible applications, Ln–A manganites now also are of particular interest and their electronic and magnetic structures are extensively studied [4–6]. The ferromagnetic (FM) state in manganites is considered to be caused by partial substitution of A^{2+} ions for Ln^{3+} ions and to be related to the exchange interaction between Mn^{3+} and Mn^{4+} in the framework of the double exchange model [7]. However, some researchers suppose that the crystal-chemical bond in Ln–Sr manganites is more complex than that assumed in the simple ionic model. In particular, the authors of [8] noted that the holes that form in such a system can be compensated due to an increase in the valence of both Mn and rare-earth elements (Ce, Pr). The possible contribution of the spins of rare-earth ions (Dy, Pr) to the total magnetization of manganites was investigated in [9–11]. Therefore, it is interesting to study manganites by X-ray absorption near-edge spectroscopy (XANES) and X-ray magnetic circular dichroism (XMCD), since these are element-sensitive methods and can be used to investigate the electronic and magnetic states of various types of atoms in complex compounds.

The purpose of this work is to study the spectral dependences of XANES and XMCD near the MnK edge and the Pr $L_{2,3}$ edges for the $Pr_{1-x}Sr_xMnO_3$ ($x = 0.2, 0.4$) films in the ferromagnetic phase. It should be noted that $Pr_{0.8}Sr_{0.2}MnO_3$ and $Pr_{0.6}Sr_{0.4}MnO_3$ represent two different types of compounds, namely, an FM insulator ($x = 0.2$) and an FM semiconductor ($x = 0.4$), which makes it possible to investigate the physics of manganites in detail.

2. EXPERIMENTAL

XANES and XMCD studies were performed on the polycrystalline $Pr_{0.8}Sr_{0.2}MnO_3$ and $Pr_{0.6}Sr_{0.4}MnO_3$ films 150 and 130 nm thick, respectively. The samples were prepared by reactive high-frequency magnetron sputtering using the facing-target scheme [12]. Stoichiometric $Pr_{0.8}Sr_{0.2}MnO_3$ and $Pr_{0.6}Sr_{0.4}MnO_3$ targets were fabricated by solid-phase synthesis using the Pr_2O_3, SrO, and MnO_2 powders. As substrates, we used single-crystal YSZ (311) yttrium-stabilized zirconium oxide. The substrate temperature in sputtering was 750°C. The investigation of the magnetic properties in [13] showed that the Curie temperature (T_C) of $Pr_{0.8}Sr_{0.2}MnO_3$ is 115 K and that of $Pr_{0.6}Sr_{0.4}MnO_3$ is

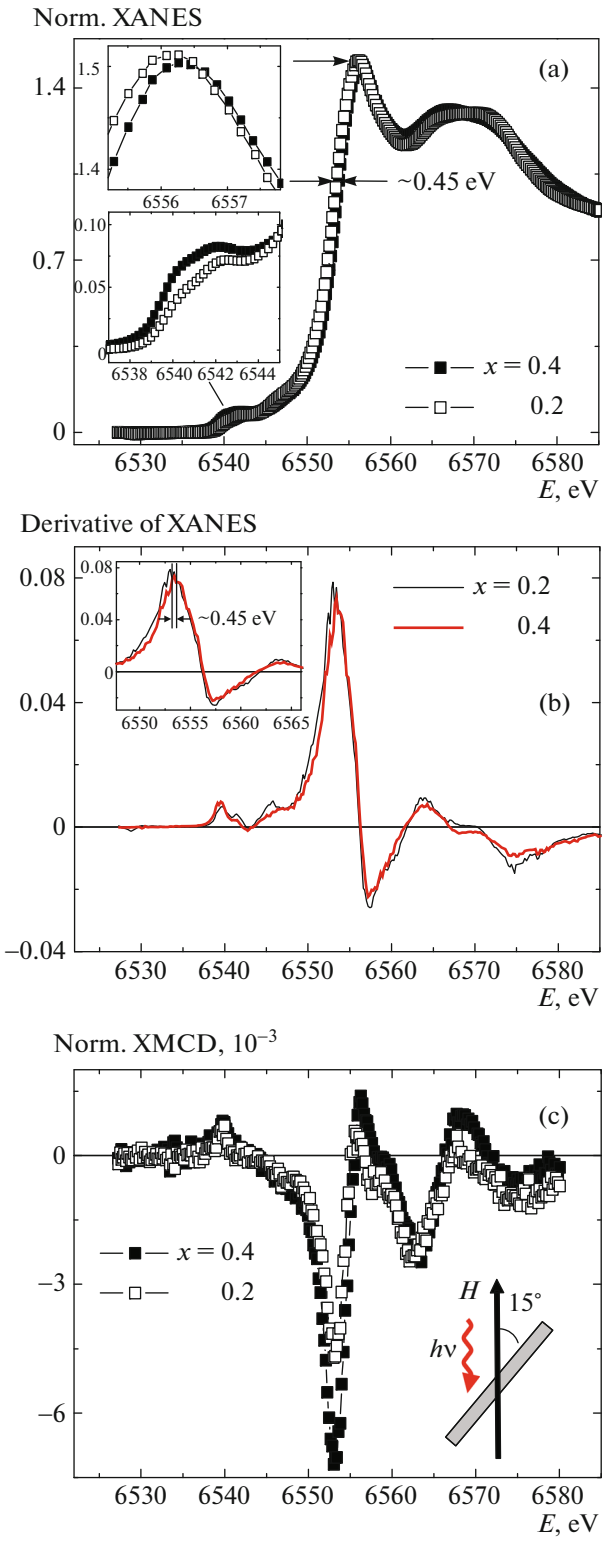

Fig. 1. (a) XANES spectra, (b) first derivative of the XANES spectra, and (c) XMCD spectra at the K edge of Mn for the $Pr_{1-x}Sr_xMnO_3$ films at $T = 90$ K. Insets: (a) main absorption peak and pre-edge structure in scale; (b) first derivative of the XANES spectra at absorption edges, and (c) XMCD measurement scheme in a magnetic field $H = 1$ T.

approximately 215 K. Therefore, XANES and XMCD spectra were recorded at $T = 90$ K, which corresponded to the FM phase of the films. Note that T_C of the bulk samples is 150 K (for $Pr_{0.8}Sr_{0.2}MnO_3$) and 300 K ($Pr_{0.6}Sr_{0.4}MnO_3$). In [13], the lower T_C value of the films was related to the inhomogeneity of the magnetic state near the phase transition temperature since the study of the crystal structure and phase homogeneity of these films in [14] revealed the presence in the samples of only one declared phase with structural parameters close to the data for the bulk $Pr_{0.8}Sr_{0.2}MnO_3$ and $Pr_{0.6}Sr_{0.4}MnO_3$ samples.

Element-sensitive XANES and XMCD measurements were carried out at the ID12 beamline at the European Synchrotron Radiation Facility. XANES spectra were recorded for right-hand (κ_{right}) and left-hand (κ_{left}) circular polarization of waves when a photon beam was incident at an angle of 15° to the sample surface at $T = 90$K in a magnetic field $\mathbf{H}^+ = 1$ T (experimental scheme is shown in Fig. 1c). A total fluorescence yield was used [15]. The experimental spectra were normalized so that the absorption jump at the edges of Mn and Pr was equal to one.

XMCD spectra were obtained as the difference between the normalized XANES spectra measured for X-ray right-hand and left-hand circular polarization. To exclude an experimental error in dichroism spectra, we also performed experiments for the opposite magnetic field direction ($\mathbf{H}^- = 1$ T). The XMCD spectra presented in this work were calculated by the formula

$$\mathrm{XMCD}(E) = \{[\kappa_{right}(E) - \kappa_{left}(E)]^{H^+}/i + [\kappa_{right}(E) - \kappa_{left}(E)]^{H^-}/j\}/2. \quad (1)$$

The field dependences of XMCD were measured at the points of the maximum dichroism value at the K edge of Mn and the L_2 edge of Pr at $T = 90$ K and $H^{\pm} = 1$ T.

3. RESULTS AND DISCUSSION

3.1. XANES and XMCD near the K Edge of Mn

Figure 1 shows the XANES and XMCD spectra of the $Pr_{1-x}Sr_xMnO_3$ films near the K edge of Mn. The $Pr_{0.8}Sr_{0.2}MnO_3$ and $Pr_{0.6}Sr_{0.4}MnO_3$ samples exhibit similar spectra, which agree well with the spectra recorded for the K edge of Mn in substituted manganites, namely, the XANES [16–19] and XMCD [20, 21] spectra. The XANES spectrum includes the main absorption peak at 6556 eV, a pre-edge structure at 6536–6550 eV, and a peak behind the main absorption line at 6562–6588 eV (which is attributed to multiple atomic scattering around absorbing Mn). The main absorption peak reflects the transition from the 1s orbitals to the 4p orbitals of Mn. When the Sr content increases, the intensity of this peak decreases and it

shifts by 0.2 eV toward high energies (inset to Fig. 1a). The absorption edge (E_0) determined from the maximum of the first derivative also shifts toward high energies by 0.45 eV (Fig. 1b). It is found that the shift by energy of both the absorption edge and the main absorption maximum in such materials are related to a change in the average oxidation degree of the absorbing atom and a change in the Mn–O bond length due to the difference between the Pr^{3+} and Sr^{2+} ion radii [16–19]. The values of E_0 for the $Pr_{0.8}Sr_{0.2}MnO_3$ and $Pr_{0.6}Sr_{0.4}MnO_3$ films are 6553.15 ± 0.008 eV and 6553.6 ± 0.018 eV, respectively, with allowance for the absolute measurement error (the average values of the XANES spectra were calculated by Eq. (1) where sign minus was replaced by plus at $i = j = 10$). We failed to find an accurate value of E_0 for the base compound $PrMn^{3+}O_3$. Nevertheless, based on the XANES spectrum in [17], the absorption edge of this compound is approximately 6553 eV. Therefore, the absorption edges of the $Pr_{1-x}Sr_xMnO_3$ films lie between the energies of the base compounds $PrMn^{3+}O_3$ (6553 eV) and $SrMn^{4+}O_3$ (6555.67 eV) [16] and significantly closer to the edge of $PrMnO_3$. This behavior points to an intermediate valence state of manganese in the films. The significant difference between the energies of the samples under study and $SrMnO_3$ is likely caused by the low concentration of tetravalent manganese in the films. At that, the difference between the values of E_0 for the $Pr_{0.8}Sr_{0.2}MnO_3$ and $Pr_{0.6}Sr_{0.4}MnO_3$ samples indicates the presence of tetravalent manganese, the content of which is higher in $Pr_{0.6}Sr_{0.4}MnO_3$.

The difference between the XANES spectra of the studied samples is also observed in the pre-edge region. The pre-edge structure forms due to the quadrupole transitions of the 1*s* electrons to the unfilled 3*d* band partly hybridized with 4*p* states of Mn [22]. When the Sr content increases, the spectral weight in this region increases. Similar behavior was observed earlier in the $La_{1-x}Ca_xMnO_3$ samples and was attributed to an increase in the hybridization of the 4*p* states of Mn with the 3*d* states of the neighboring Mn ions [22–24].

As the absorption spectrum, the XMCD spectrum has a resonance band at the absorption edge, a maximum in the pre-edge region, and a maximum in the post-edge region. In this case, the XMCD signal at the absorption edge has a dispersion shape. These spectral features are characteristic of both samples. Only the increase in their intensity in the sample with a high content of Sr is worth noting. XMCD at the absorption *K* edge is known to be related to the orbital magnetic moment of the *p* states of an absorbing atom. The spin polarization of the 4*p* states appears in Mn atoms due to the exchange interaction with the spin-polarized 3*d* band, which is responsible for the magnetism of the samples [25]. Thus, changes in the 3*d* polarization are reflected in XMCD at the *K* edge because of spin–orbit coupling. The increase in the XMCD intensity of the $Pr_{0.6}Sr_{0.4}MnO_3$ film points to a growth of the total magnetic moment of the sample due to an increase in the 4*p*–3*d* hybridization. This statement is confirmed by the magnetic moments of the films in the saturation state that were obtained in [26] for the films $Pr_{0.8}Sr_{0.2}MnO_3$ (M_S ~ 1.66μ_B/formula unit and 3μ_B/formula unit) and $Pr_{0.6}Sr_{0.4}MnO_3$ (M_S ~ 2.29μ_B/formula unit and 3.2μ_B/formula unit) from the magnetization curves recorded at T = 5 and 90 K, respectively. Moreover, the $Pr_{0.6}Sr_{0.4}MnO_3$ film demonstrates a decrease in the XANES signal intensity in the range of the main absorption peak, which also implies a decrease in the density of the 4*p* states by increasing 4*p*–3*d* hybridization.

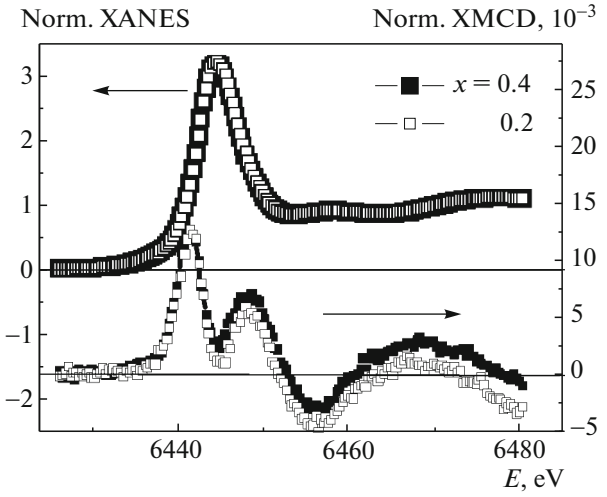

Fig. 2. XANES and XMCD spectra at the L_2 edge of Pr for the $Pr_{1-x}Sr_xMnO_3$ films at T = 90 K in a magnetic field H = 1 T (for XMCD).

3.2. XANES and XMCD near the $L_{2,3}$ Edges of Pr

The XANES and XMCD spectra of the films under study near the $L_{2,3}$ edges of Pr are shown in Figs. 2 and 3. The XANES spectra of both $Pr_{1-x}Sr_xMnO_3$ samples almost coincide at the L_2 and L_3 edges. Their spectral shape also agrees well with the data in [18, 27–29].

The spectral features of XMCD are also similar for both samples. The spectra recorded near the L_2 edge (Fig. 2) resemble the spectra of Ce in $CeFe_2$ [30] and Eu in EuN [31], which have two peaks related to a mixed valence state of a rare-earth ion at the absorption edge. Moreover, two peaks are also observed in the pre-edge region in the XMCD spectra of the films. The XMCD spectrum near the L_3 edge differs from that near the L_2 edge (Fig. 3). Such a shape with a predominant maximum in the positive region of the spectrum is close to the XMCD of Tb at the L_3 edge in

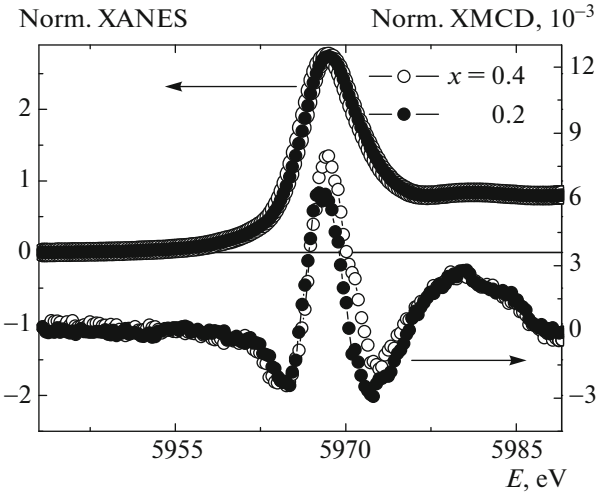

Fig. 3. XANES and XMCD spectra at the L_3 edge of Pr for the $Pr_{1-x}Sr_xMnO_3$ films at $T = 90$ K in a magnetic field $H = 1$ T (for XMCD).

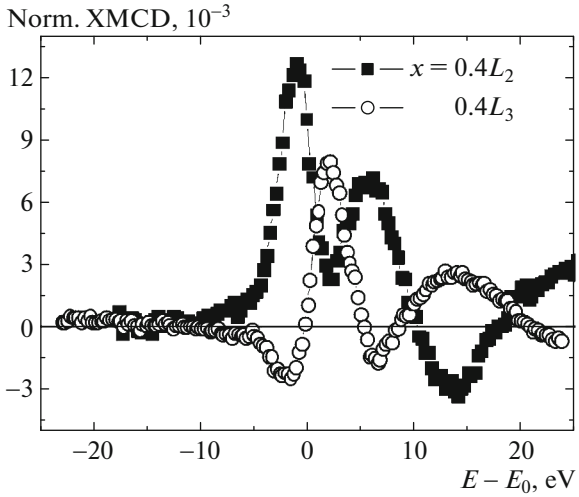

Fig. 4. XMCD spectra at the $L_{2,3}$ edges of Pr for the $Pr_{0.6}Sr_{0.4}MnO_3$ film at $T = 90$ K and $H = 1$ T.

$La_{0.67-y}Tb_yCa_{0.33}MnO_3$ [21]. According to the selection rules, the $2p_{1/2} \rightarrow 5d_{3/2}$ dipole transitions make the main contribution to the L_2-edge absorption and the $2p_{3/2} \rightarrow 5d_{5/2}$ transitions make the main contribution to the L_3-edge absorption (a weak contribution from the $2p_{1/2} \rightarrow 5d_{3/2}$ transitions is also observed). Obviously, the two peaks in the XMCD spectra near the L_2 edge are associated with the mixed valence of praseodymium. The center distance between these peaks is approximately 7 eV, which agrees with the XMCD data at the L_2 edge of Eu in EuN containing Eu^{2+} ($4f^7$) and Eu^{3+} ($4f^6$) ions [31]. Such a difference in the XMCD spectrum at the L_2 edge of Ce in $CeFe_2$ containing Ce^{3+} ($4f^1$) and Ce^{4+} ($4f^0$) reaches 11 eV [30]. Thus, the low-energy peak can be attributed to Pr^{3+} ($4f^2$) and the high-energy peak, to Pr^{4+} ($4f^1$). The XMCD spectrum analysis near the L_3 edge is more complex. Based on the experimental and theoretical investigations of rare-earth compounds, it can be assumed that, in the presence of $4f$ electrons (beginning from Ce, $4f^1$), the crystal field most significantly affects the L_3 edge [32]. For clarity, we present the XMCD spectra at the $L_{2,3}$ edges of the $Pr_{0.6}Sr_{0.4}MnO_3$ film in one graph (Fig. 4). As in the case of Mn, the absorption edge energy (E_0) of the spectra was determined by the maximum of the first derivative of the XANES spectra. As is seen in Fig. 4, the positions of the extrema of the L_2 and L_3 edges coincide (without regard for the pre-edge structure). At that, the XMCD signals at these points have opposite signs. Such a coincidence suggests that the spectral features of the L_3 edge also reflect the mixed valence of praseodymium; however, the true cause of these features is not obvious. Note only that upon a transition to the sample with a high Sr content, the XMCD spectra near $L_{2,3}$ edges are changed in the regions related to the $4f^1$ states of Pr.

The appearance of the Pr^{4+} ions in the $Pr_{1-x}Sr_xMnO_3$ ($x \le 0.5$) films is likely caused by a strong Pr($4f$)–O($2p$) interaction and the existence of holes in the $2p$ states of oxygen. The localization of holes at O($2p$) in $La_{1-x}Sr_xMnO_3$ was experimentally supported by X-ray spectroscopy at the K edge of oxygen [33]. The hybridization of the Pr($4f$)–O($2p$) orbitals was detected in $Pr_{1-x}Sr_xMnO_3$ and explained by small Pr–O interionic distances [34]. The presence of Pr^{4+} was assumed in the $Pr_{0.5}Ca_{0.5}CoO_3$ system [28]. The change in the valence from Pr^{3+} to Pr^{4+} was attributed to $4f$-electron delocalization due to a strong Pr($4f$)–O($2p$) interaction and the possible charger-transfer electron transition $Pr^{3+} \rightarrow O \rightarrow Co^{4+}$. Probably due to the transition $Pr^{3+} \rightarrow O \rightarrow Mn^{4+}$ in the studied films (with an increase in x), there is only the small shift of the K-edge absorption of Mn in the XANES spectra. However, the additional temperature measurements of XMCD at the L_2 edge of Pr are required to reveal this transition in the $Pr_{1-x}Sr_xMnO_3$ system.

3.3. Field Dependence of XMCD near the K Edge of Mn and the L_2 Edge of Pr

Figure 5 shows the field dependences of the XMCD signal measured at the points of the maximum dichroism at the K edge of Mn (6553 eV) and the L_2 edge of Pr value (6441 eV) for the $Pr_{0.8}Sr_{0.2}MnO_3$ and $Pr_{0.6}Sr_{0.4}MnO_3$ films. The field dependences of XMCD at the K edge of Mn demonstrate symmetric hysteresis loops with a magnetic saturation field of about 0.2 T for both samples. However, the field dependences of XMCD obtained at the L_2 edge of Pr

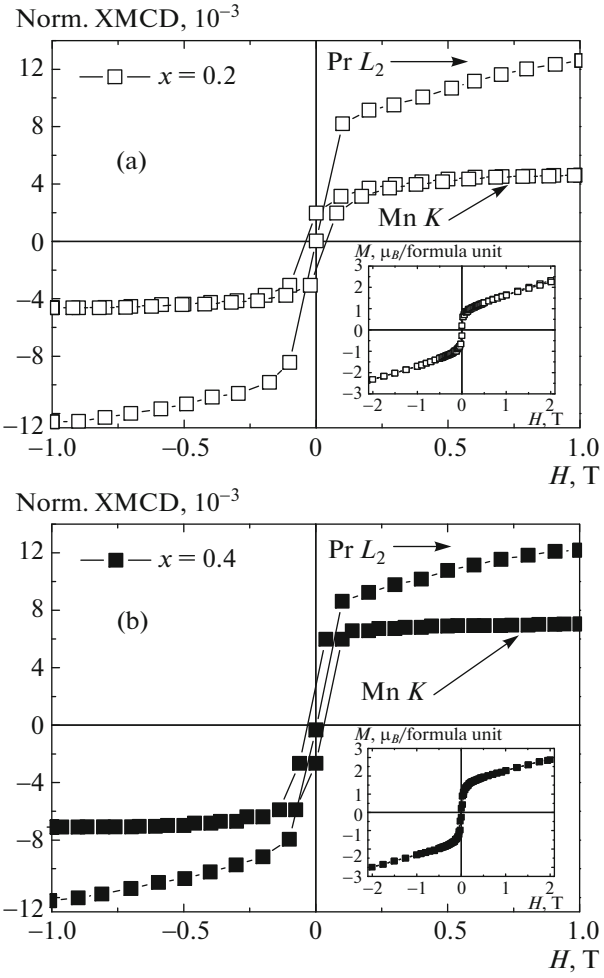

Fig. 5. Field dependences of XMCD at the K edge of Mn (6553 eV) and the L_2 edge of Pr (6441 eV) for the $Pr_{0.8}Sr_{0.2}MnO_3$ (a) and $Pr_{0.6}Sr_{0.4}MnO_3$ (b) film at T = 90 K. Inset: field dependences of the magnetization of the same samples at T = 90 K (diamagnetic contribution from the substrate was deducted).

are symmetric curves passing through zero. The linear part of these curves, which is reminiscent of the approach to magnetic saturation, is attributed to the Van Vleck paramagnetism of Pr^{3+} ions; this makes a significant contribution to the total magnetization of the samples as can be seen in the inserts of Fig. 5. The magnetization curves measured at T = 90 K in the same magnetic fields look like the sum of the XMCD(H) curves recorded at the K edge of Mn and the L_2 edge of Pr.

4. CONCLUSIONS

Thus, according to XANES and XMCD spectroscopy, the mixed valence state of Mn ($3d^4$, $3d^3$) and Pr ($4f^2$,$4f^1$) was revealed in the $Pr_{0.8}Sr_{0.2}MnO_3$ and $Pr_{0.6}Sr_{0.4}MnO_3$ films. The observed $4f^1$ state of Pr in the films implies the presence of vacancies in the $2p$ states of oxygen and the possible charge-transfer transition $Pr^{3+} \rightarrow Mn^{4+}$. The XMCD data point to ferromagnetic behavior of Mn ions and the Van Vleck paramagnetism of Pr ions, which makes a significant contribution to the total magnetization of the films. The main difference between the samples is most pronounced in the XMCD spectra at the K edge of Mn, which indicates a growth of the total magnetic moment with an increase in Sr substitution.

ACKNOWLEDGMENTS

We thank V.I. Chichkov and N.V. Andreev (National University of Science and Technology MISiS) for the preparation of the manganite films.

This work was supported by the Russian Foundation for Basic Research (project no. 16-32-00209 mol_a) and a grant of the President of the Russian Federation (NSh-7559.2016.2).

REFERENCES

1. A.-M. Haghiri-Gosnet and J.-P. Renard, J. Phys. D: Appl. Phys. **36**, R127 (2003).
2. C. Moreno, C. Munuera, S. Valencia, et al., Nano Lett. **10**, 3828 (2010).
3. N. V. Volkov, Phys. Usp. **55**, 250 (2012).
4. B. S. Nagaraja, A. Rao, and G. S. Okram, J. Alloys Compd. **683**, 308 (2016).
5. T. I. Arbuzova and S. V. Naumov, JETP Lett. **101**, 760 (2015).
6. Hong Sub Lee, Sun Gyu Choi, Hyung-Ho Park, et al., Sci. Rep. **3**, 1704 (2013).
7. C. Zener, Phys. Rev. **82**, 403 (1951).
8. A. E. Sovestnov, A. V. Tyunis, E. V. Fomin, A. A. Petrunin, A. I. Kurbakov, and B. T. Melekh, Tech. Phys. Lett. **35**, 26 (2009).
9. J. Dho, W. S. Kim, E. O. Chi, et al., Solid State Commun. **125**, 143 (2003).
10. B. Padmanabhan, S. Elizabeth, H. L. Bhat, et al., J. Magn. Magn. Mater. **307**, 288 (2006).
11. S. Rößler, S. Harikrishnan, U. K. Rößler, et al., J. Phys.: Conf. Ser. **200**, 012168 (2010).
12. Y. Hoshi, M. Kojima, M. Naoe, et al., Electron. Commun. Jpn., Pt. I **65**, 91 (1982).
13. Yu. E. Samoshkina, M. V. Rautskii, E. A. Stepanova, D. S. Neznakhin, N. V. Andreev, and V. I. Chichkov, J. Exp. Theor. Phys. **125**, 1090 (2017).
14. I. Edelman, Yu. Greben'kova, A. Sokolov, et al., AIP Adv. **4**, 057125 (2014).
15. A. Rogalev and F. Wilhelm, Phys. Met. Metallogr. **116**, 1285 (2015).
16. S. K. Pandey, R. Bindu, A. Kumar, et al., Pramana – J. Phys. **70**, 359 (2008).
17. Q. Qian, T. A. Tyson, C.-C. Kao, et al., Phys. Rev. B **64**, 024430 (2001).

18. T.-Y. Tan, N. Martin, Q. Zhou, et al., J. Solid State Chem. **201**, 115 (2013).
19. Z. W. Ouyang, Y. H. Matsuda, H. Nojiri, et al., J. Phys.: Condens. Matter **21**, 016006 (2009).
20. G. Subías, J. García, M. G. Proietti, et al., Phys. Rev. B **56**, 8183 (1997).
21. M. Sikora, Cz. Kapusta, D. Zając, et al., J. Alloys Comp. **328**, 100 (2001).
22. F. Bridges, C. H. Booth, G. H. Kwei, et al., Phys. Rev. B **61**, R9237 (2000).
23. A. Yu. Ignatov, N. Ali, and S. Khalid, Phys. Rev. B **64**, 014413 (2001).
24. J. García, M. C. Sánchez, G. Subías, et al., J. Phys.: Condens. Matter **13**, 3229 (2001).
25. Y. Ding, D. Haskel, Y.-Ch. Tseng, et al., Phys. Rev. Lett. **102**, 237201 (2009).
26. Yu. E. Samoshkina, I. S. Edelman, E. A. Stepanova, et al., J. Magn. Magn. Mater. **428**, 43 (2017).
27. I. A. Sluchinskaya, A. I. Lebedev, and A. Erko, Phys. Solid State **54**, 975 (2012).
28. J. Herrero-Martín, J. L. García-Muñoz, S. Valencia, et al., Phys. Rev. B **84**, 115131 (2011).
29. H. Asakura, T. Shishido, Sh. Fuchi, et al., J. Phys. Chem. C **118**, 20881 (2014).
30. F. Baudelet, Ch. Giorgetti, S. Pizzini, et al., J. Electron. Spectrosc. Relat. Phenom. **62**, 153 (1993).
31. B. J. Ruck, H. J. Trodahl, J. H. Richter, et al., Phys. Rev. B **83**, 174404 (2011).
32. C. Neumann, B. W. Hoogenboom, A. Rogalev, et al., Solid State Commun. **110**, 375 (1999).
33. E. Pellegrin, L. H. Tjeng, F. M. F. de Groot, et al., J. Electron Spectrosc. **86**, 115 (1997).
34. J.-S. Kang, T. W. Noh, C. G. Olson, et al., J. Electron Spectrosc. **114–116**, 683 (2001).
35. K. Fukui, H. Ogasawara, A. Kotani, et al., Phys. Rev. B **64**, 104405 (2001).

Translated by K. Shakhlevich